

## **Retreat of a giant cataract in a long-lived (3.7 Ga – 2.6 Ga) martian outflow channel**

\*Nicholas Warner<sup>1</sup>, Sanjeev Gupta<sup>1</sup>, Jung-Rack Kim<sup>2</sup>, Shih-Yuan Lin<sup>2</sup> and Jan-Peter Muller<sup>2</sup>

<sup>1</sup>*Dept. Earth Science & Engineering, Imperial College London, South Kensington Campus,*

*London, SW7 2AZ, <sup>2</sup>Mullard Space Science Laboratory, Department of Space and Climate*

*Physics, University College London, Holmbury St Mary, Surrey, RH5 6NT*

\* Email: n.warner@imperial.ac.uk

### **GSA DATA REPOSITORY**

#### **Data Repository Methods**

1. HRSC Digital Terrain Model construction methods
2. CTX Digital Terrain Model construction methods
3. Assessment of DTM height accuracy
4. Crater Count Methods

#### **Data Repository Figures**

Figure DR1: Plots of CTX stereo DTM (all height grid-points) (red line) compared against the MOLA height points (black crosses).

Figure DR2: Plots of CTX (red) and HRSC stereo DTM (green) (all height grid-points) compared against the MOLA height points (black cross).

Figure DR3: MOLA shaded relief map of the Ares Vallis region displaying major geographic features in the study.

Figure DR4: HIRISE image of the cataract displaying the longitudinal grooves on the upper surface and the small amphitheater head-cuts along the cataract lip.

Figure DR5: Example impact craters from the upper and lower surfaces of the cataract. a, Post-flood impact craters on  $S_u$ . b, c Example pre-flood modified impact craters and non-modified post-flood craters on  $S_u$ . d, Example post-flood impact craters on  $S_l$ .

Figure DR6: CTX image P06\_003538\_1883 displaying counts on  $S_u$  and  $S_l$ .

Table DR1: Crater statistics for the upper ( $S_u$ ) and lower ( $S_l$ ) surfaces of the cataract tributary to Ares Vallis.

## Data Repository Methods

### ***1. HRSC Digital Terrain Model construction methods***

To describe the morphology of the medial Ares Vallis outflow channel and associated tributary channel we used a newly created HRSC DTM with 70 m grid-spacing. Comparisons with MOLA height profiles indicate  $\pm 25$  m vertical accuracy and zero bias [Warner *et al.*, 2009]. The HRSC DTM of medial Ares Vallis was created based on the MOLA DTM after refinement using the surface matching technique [Lin *et al.*, 2010]. Further refinement of the DTM was done using the iterative feed-forward technique [Kim and Muller, 2009] and was stereo noise reduced using the method of Lin *et al.* (2008). These high resolution (50-75 m) DTMs have been created using a unique processing system developed at UCL [Kim and Muller, 2009] which is also described in Warner *et al.* (2009).

### ***2. CTX Digital Terrain Model construction methods***

The NASA MRO (Mars Reconnaissance Orbiter) deploys two optical pushbroom CCD (Charge Couple Device) cameras that are capable of across-track stereo targeting. Both the CTX (Context Camera) and HiRISE (High Resolution Imaging Science Experiment) provide very high-resolution imagery at 6 m and sub-metre (up to 20 cm) resolution respectively [Kirk *et al.*, 2008; Malin *et al.*, 2007]. For some 10% of the total acquisitions, across-track stereoscopic observations can be acquired by HiRISE with a slightly higher (as yet unpublished) duty cycle from CTX. Digital Terrain Model (DTM) creation from HiRISE was first published by Kirk *et al.* [Kirk *et al.*, 2008]. Then Kim and Muller (2009) successfully developed a processing method for the multi resolution DTMs from HSRC-CTX-HIRISE stereo overlap. This uses a 3D zooming method employing a non-rigorous sensor model and hierarchical geometric control. Here, we only use the CTX DTM extraction techniques with HRSC base control information. Further technical details are presented in [Kim and Muller, 2008].

The target study area of this paper is covered by a CTX stereo pair: P06\_003538\_1883 and P08\_004171\_1883. The high SNR (signal to noise ratio > 100:1) [Malin *et al.*, 2007] and relatively high IFOV (Instantaneous Field of View) of the CTX pair results in a very high coverage of successful stereo image matches producing a very dense and low noise disparity map for an output 18 m stereo DTM. However, the long exposure time of CTX image pairs creates difficulties for the photogrammetric sensor modelling. In general, such inaccuracy in the sensor model causes significant vertical and horizontal shifts especially at the boundaries of the target image pair. We tackled this problem in two ways: 1) by use of a non-rigorous sensor model for the relatively small stereo coverage in order to smoothly interpolate the pointing errors; and 2) by iterative establishment of a sensor model using the HRSC DTM as the reference plane (see technical details in [Kim and Muller, 2008; 2009]).

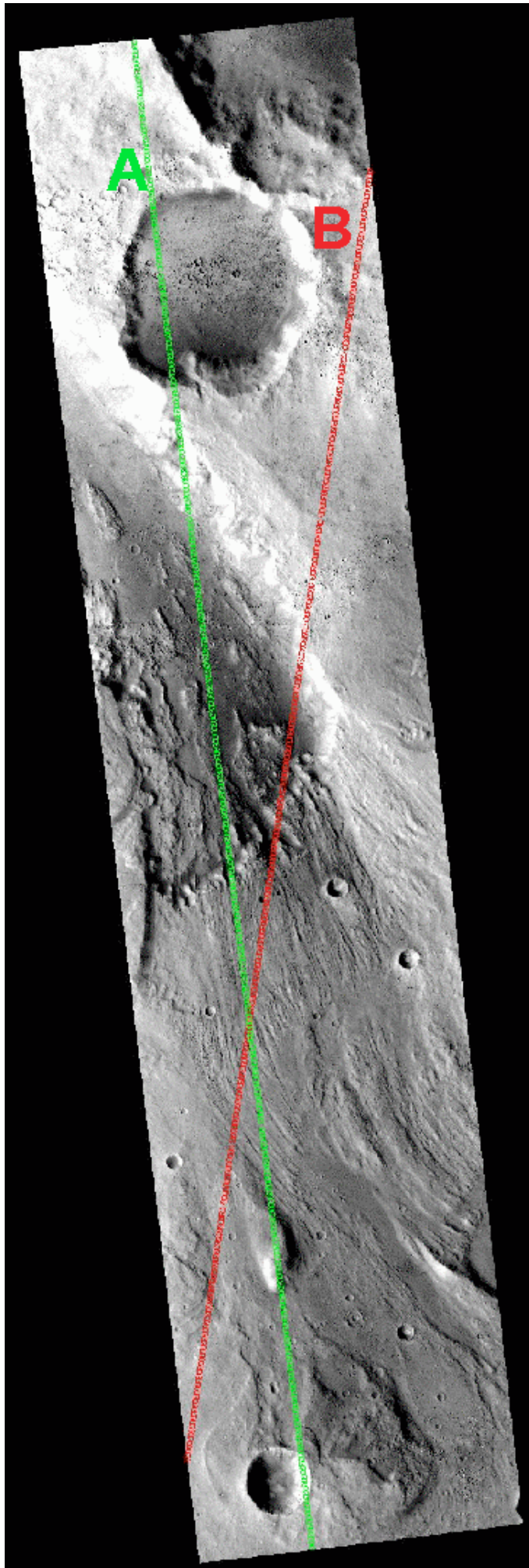
The final DTM product compared with MOLA spot elevations shows a reasonable agreement with the MOLA height profile (see below). The DTM has a grid-spacing of 18 m, and we propose that the theoretical vertical precision is approximately several meters considering our sub-pixel image matching accuracy. However, realistically the vertical accuracy of the CTX DTM requires verification compared against a higher resolution DTM profile such as HiRISE. The results of such comparisons over some sample sites were demonstrated in Kim and Muller [Kim and Muller, 2009] and showed less than 16 m standard deviation. Large portion of such errors are likely a result of geodetic control errors so that we are confident that the relative height accuracy between CTX height points is within several metres level.

### **3. Assessment of DTM height accuracy**

The photogrammetric accuracy assessment of HRSC topographic products has been investigated and verified [Spiegel, 2007]. In this paper, the MOLA height spots corrected for bad orbits and occasional biases [Neumann *et al.*, 2001] were employed to validate the CTX

stereo DTM. There are 6, 700 MOLA spots and 63 tracks within target area. The mean height difference between MOLA-CTX is -0.37 m with a standard deviation of 49.628 m. The two profiles crossing the central areas are shown in Figure DR1.

In these profiles, the CTX DTM shows very good agreement with MOLA spots in general but the deviation in some rough surface may result from the influence of the MOLA spot's footprint size (160 m). In addition, there is some noise due to stereo matching over some areas such as crater walls, which leads to a height difference between MOLA. Compared with HRSC DTMs, it is very clear that the CTX DTM shows much more detail in topography (see Figure DR2). The problem with the CTX DTM is that the non-rigorous sensor model produced a somewhat significant error offset at the along-track end of the stereo images. This effect was shown in both the extreme end portion of profile B, which contributes to the relatively high standard deviation of the MOLA-CTX DTM. However, these do not affect the topographic analysis of this research.





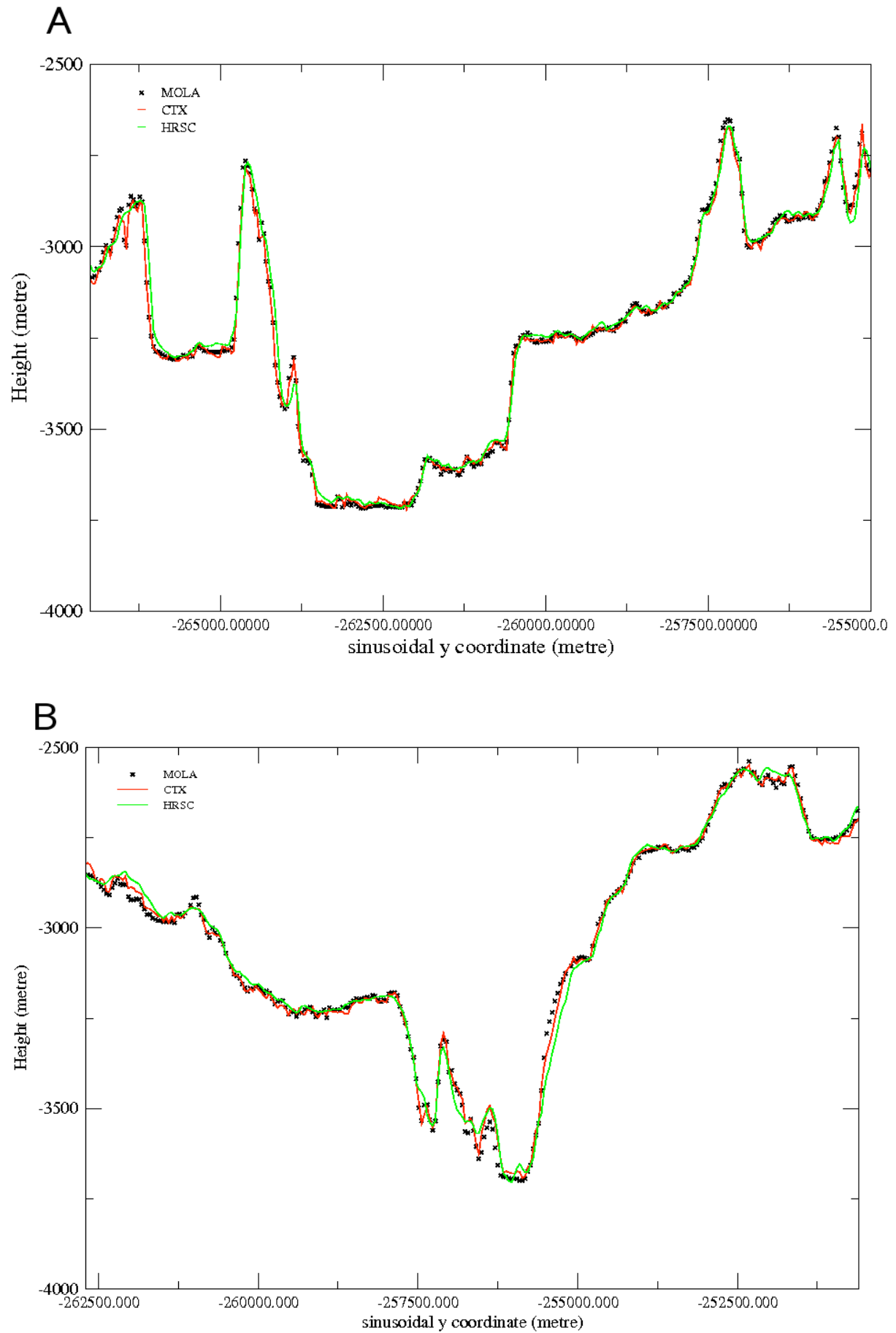


**Figure DR2: Plots of CTX (red) and HRSC stereo DTM (green) (all height grid-points) compared against the MOLA height points (black cross).**

#### 4. Crater Count Methods

To refine the timing of flood events within the tributary canyon and Ares Vallis (Figs. DR3, DR4) we obtained crater counts for  $D$  (diameter)  $> 100$  m from high-resolution ( $6 \text{ m pix}^{-1}$ ) MRO context camera images (CTX). Counts were made using the Mars Editing and Assessment toolset [Simpson *et al.*, 2008] using two CTX images for  $S_u$  (P06\_003538\_1883,

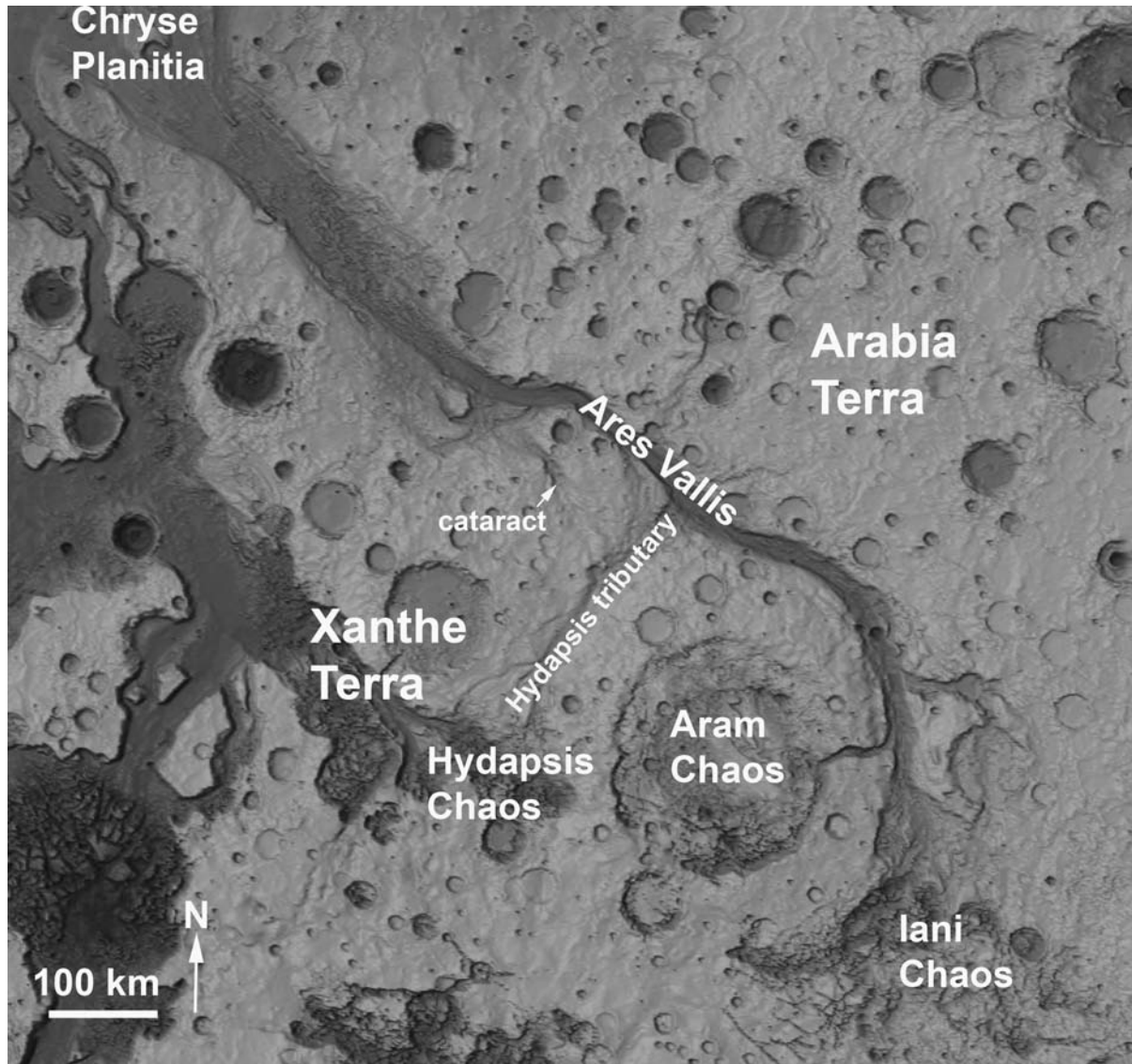


**Figure DR3: MOLA shaded relief map of the Ares Vallis region displaying major geographic features in the study.**

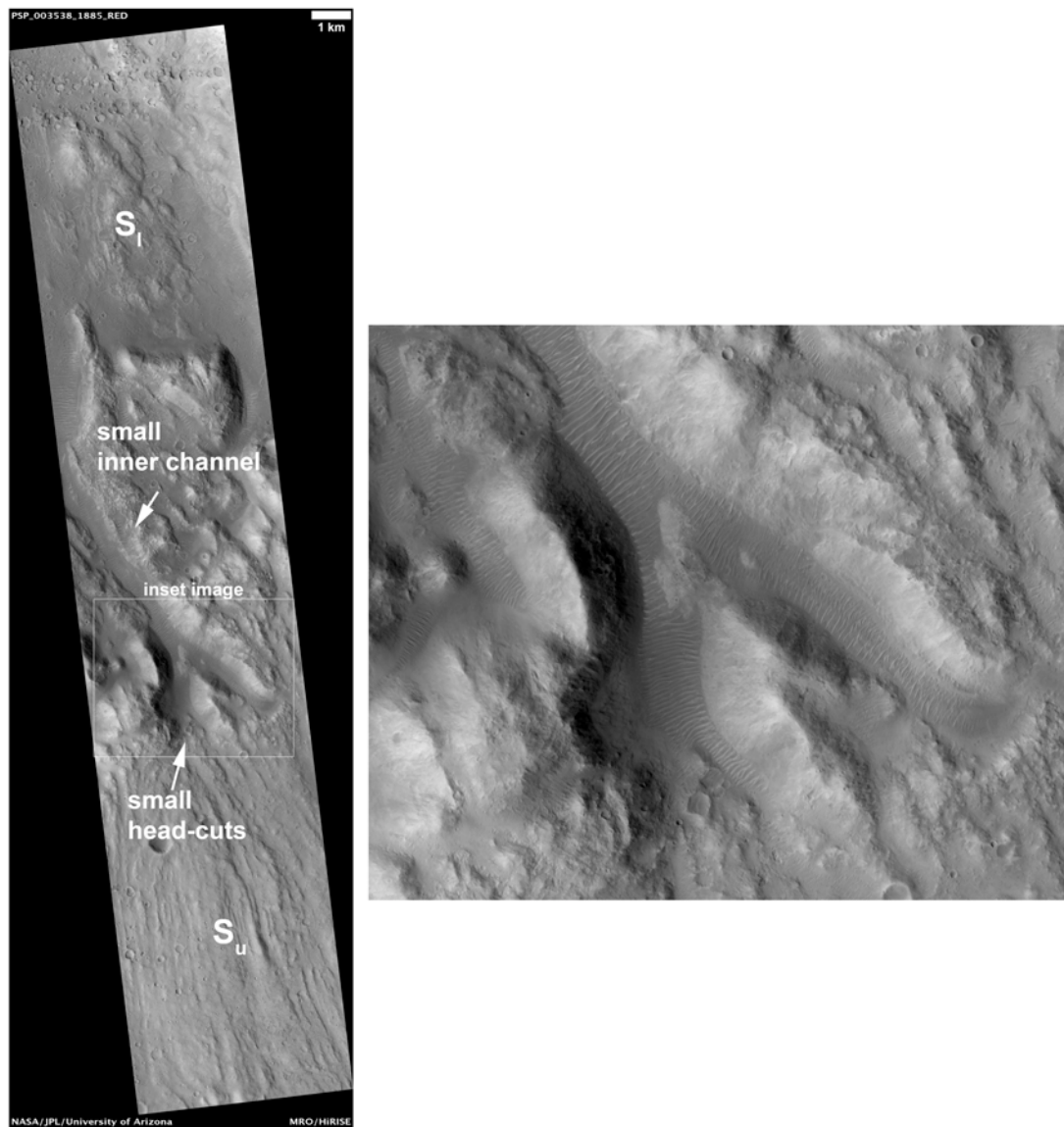


**Figure DR4: HIRISE image of the cataract displaying the longitudinal grooves on the upper surface and the small amphitheater head-cuts along the cataract lip.**

P08\_004171\_1883), three CTX images for  $S_1$  (P06\_003538\_1883, P08\_004171\_1883, P15\_007085\_1902) and all available CTX images that were present at the time of writing of this manuscript for the main western branch canyon of Ares Vallis extending from a latitude of  $1.3^\circ$  N at Iani Chaos to  $14.2^\circ$  N near the mouth of Ares Vallis. Figure DR5 displays CTX images showing post-flood and pre-flood impact crater populations on the

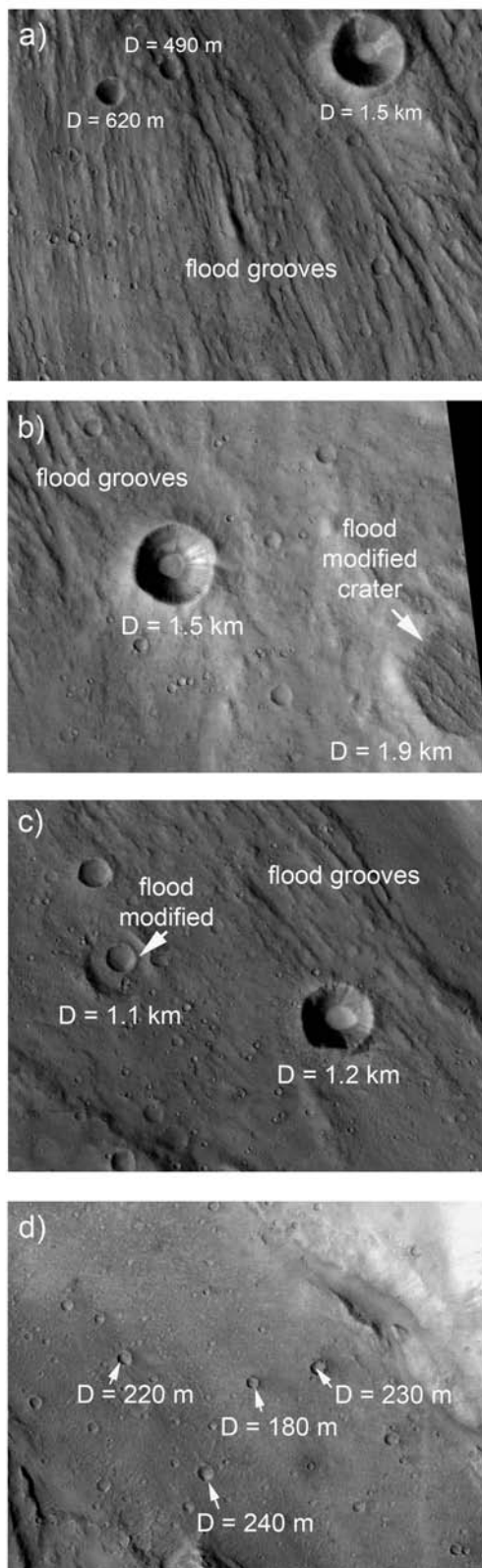


**Figure DR5: Example impact craters from the upper and lower surfaces of the cataract. a, Post-flood impact craters on  $S_u$ . b, c Example pre-flood modified impact craters and non-modified post-flood craters on  $S_u$ . d, Example post-flood impact craters on  $S_l$ .**

tributary channel surface. Figure DR6 displays an example CTX image with an overlay of the shape file of a portion of the counted craters for  $S_u$  and  $S_l$ . The crater count toolset is a visual

basic application that allows craters to be tagged and measured on an image mosaic backdrop (at full resolution), saving relevant diameter and location data to an ESRI shapefile. For this analysis, all randomly distributed impact craters on the flood surfaces were counted. Non-randomly distributed secondary craters found in chains or clusters were excluded. Several obvious secondary crater ejecta rays occur across the southern portion of  $S_u$  (including the flood terrain visible on adjacent CTX strips proximal to the Hydapsis tributary to Ares Vallis) and in limited regions on northern  $S_l$ . These regions of each surface were excluded from the analysis. Most recently, it has been established that the majority of randomly distributed impact craters with  $D > 100$  m are primary in origin with limited contamination by secondary craters [Hartmann, 2007; Hartmann et al., 2008]. It was concluded by these authors that relative and model age determination from this impact crater population is a useful method for surfaces with limited aerial exposure and limited abundance of large diameter impact craters. The total counts and counted area for our study are 16,144 and 24,642 km<sup>2</sup> respectively (excluding the  $D > 5$  km counts of the highland terrain) with the lowest number of counts (664) obtained from  $S_l$ . Counts on the lower surface are limited by the availability of CTX images. Crater statistics are presented on log<sub>10</sub> binned crater cumulative frequency plots after Hartmann and Neukum [2001] in the main text and in table form here (Table DR1) as crater densities for N(0.1), N(0.5), N(1), and N(8.0) (where N represents the cumulative number of craters counted per 10<sup>6</sup> km<sup>2</sup>). The freeware program Craterstats was used to plot the crater statistics and to fit isochrons (with error) to determine the absolute age of the flood

surfaces [Michael and Neukum, 2008]. We utilized the production and chronology functions

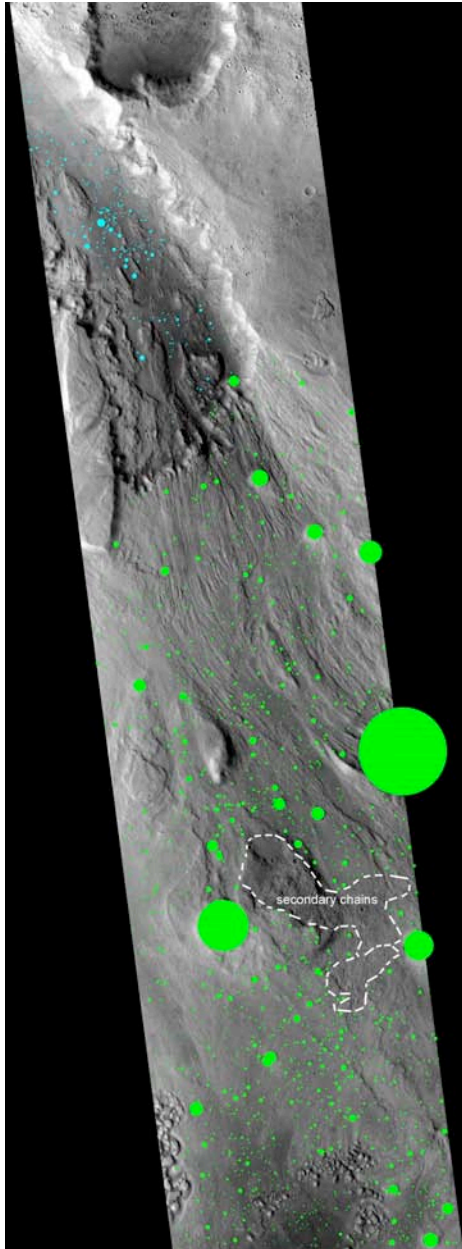


**Figure DR6: CTX image P06\_003538\_1883 displaying counts on  $S_u$  and  $S_l$ .**

Ivanov et al. [2001] and Hartmann and Neukum [2001], made available in the Craterstats program, to provide model ages for the flood erosion surfaces. On surfaces that show evidence for resurfacing (large kink in the cumulative frequency curve), a resurfacing correction for the given diameter range was applied in Craterstats following the methods described by [Michael and Neukum, 2008]. As an example, the main channel of Ares Vallis has a large kink in the cumulative frequency curve at  $D < 2$  km, which we interpret as caused

**Table DR1: Crater statistics for the upper ( $S_u$ ) and lower ( $S_l$ ) surfaces of the cataract tributary to Ares Vallis, for the main channel of Ares Vallis, and for the highland terrain surrounding the tributary canyon.**

Surface	Area (km <sup>2</sup> )	Counts	N(0.1)	N(0.5)	N(1.0)	N(8.0)	Pre-Flood Model Age, Ga	Model Age Flood events, Ga
$S_u$	2183	1699	$7.8 \times 10^5$	$2.1 \times 10^4$	$7.3 \times 10^3$	$4.6 \times 10^2$	3.87 +0.06 / -0.12	3.72 +0.04, -0.06, 2.67 +0.23, -0.25
$S_l$	739	664	$9.0 \times 10^5$	$1.5 \times 10^4$	N/A	N/A	N/A	2.63 +0.35 / -0.41
Ares Vallis	21720	13781	$6.3 \times 10^5$	$1.4 \times 10^4$	$2.5 \times 10^3$	$1.8 \times 10^2$	N/A	3.73 +0.04 / -0.05, 2.54 +0.13 / -0.13
Highland Craters	24109	17	N/A	N/A	N/A	$3.3 \times 10^2$	3.94 +0.03 / -0.04	N/A

**The cumulative number (N) of impact craters per million km<sup>2</sup> is illustrated for D = 0.1, 0.5, 1.0, and 8.0 km along with model ages for the pre-flood surface and specific flood events.**

by resurfacing of the smaller diameter craters by flood erosion. We applied a resurfacing correction for the smaller diameter craters that closely follow an isochron, which for Ares Vallis includes the craters within a diameter range of D = 300 m – 1 km. For craters with D < 300 m, dust cover and obliteration of smaller impact craters by modern Mars weathering and erosion processes (e.g. wind scour, mass wasting) cause the slope of the data to gradually dip beneath the isochron. This is confirmed for all small diameter craters in the Ares Vallis region from CTX images, particularly in proximal Ares Vallis where craters with D < 300 m show near complete dust infill. We therefore did not include this population in our resurfacing correction as this crater population would provide an anomalously low model age.

**GSA Data Repository References**

- Hartmann, W. K. (2007), Martian cratering 9: Toward resolution of the controversy about small craters, *Icarus*, 189(1), 274-278.
- Hartmann, W. K., et al. (2008), Confirmation and utilization of the "production function" size-frequency distributions of Martian impact craters, *Geophysical Research Letters*, 35(2), DOI: 10.1029/2007gl031557.
- Kim, J.-R., and J.-P. Muller (2008), Very high-resolution stereo DTM extraction and its application to surface roughness estimation over Martian surface., *International Archives of Photogrammetry, Remote Sensing and Spatial Information Sciences*, 37(B4), 993-998.
- Kim, J.-R., and J.-P. Muller (2009), Multi-resolution topographic data extraction from Martian stereo imagery, *Planetary and Space Science*, 57, 2095-2112.
- Kirk, R. L., et al. (2008), Ultrahigh resolution topographic mapping of Mars with MRO HiRISE stereo images: Meter-scale slopes of candidate Phoenix landing sites, *Journal of Geophysical Research-Planets*, 113, DOI: E00a24 10.1029/2007je003000.
- Lin, S. Y., et al. (2010), An assessment of surface matching for the automated co-registration of MOLA, HRSC and HiRISE DTMs., *Earth and Planetary Science Letters*, doi: 10.1016/j.epsl.2009.12.040, DOI: 10.1016/j.epsl.2009.12.040
- Malin, M. C., et al. (2007), Context Camera Investigation on board the Mars Reconnaissance Orbiter, *Journal of Geophysical Research-Planets*, 112(E5), DOI: 10.1029/2006je002808.
- Neumann, G. A., et al. (2001), Crossover analysis of Mars Orbiter Laser Altimeter data, *Journal of Geophysical Research-Planets*, 106(E10), 23753-23768.
- Simpson, J. I., et al. (2008), 3D crater database production on Mars by automated crater detection and data fusion, in *The International Congress of the Photogrammetry, Remote Sensing and Spatial Information Sciences*, edited, pp. 1049-1054, Beijing.
- Spiegel, M. (2007), Improvement of Interior and Exterior Orientation of the Three Line Camera HRSC with a Simultaneous Adjustment, paper presented at International Archives of Photogrammetry and Remote sensing.
- Warner, N., et al. (2009), A Refined Chronology of Catastrophic Outflow Events in Ares Vallis, Mars, *Earth and Planetary Science Letters*, doi:10.1016/j.epsl.2009.09.008.